WARSAW UNIVERSITY OF TECHNOLOGY Index 351733
FACULTY OF CIVIL ENGINEERING
COMMITTEE FOR CIVIL AND WATER ENGINEERING
POLISH ACADEMY OF SCIENCES ISSN 1230-2945

DOI: 10.24425/ace.2026.157466
ARCHIVES OF CIVIL ENGINEERING
Vol. LXXII ISSUE 1 2026
pp. 151–167

Research paper

Seismic fragility analysis of bridge structures based on improved cloud method

Ao Lu[1], Chunhua Zhang[2], Fang Huang[3], Shuang Wang[4], Ying Liu[5], Zi Wu[6]

Abstract: The cloud image method is widely used in the result vulnerability analysis because of its convenient calculation. However, there are some problems in the cloud image method, such as the engineering demand parameter (EDP) does not meet the lognormal distribution, the seismic intensity index ln(IM) does not meet the linear relationship with the engineering demand parameter (ln(EDP)), and the residual does not meet the normal distribution. Therefore, this paper introduces two methods of Box–Cox transform and 3-sigma criterion, and combines Latin hypercube sampling to propose a vulnerability analysis method that not only maintains the advantages of less analysis times of the cloud image method but also improves the normality of ln(EDP), the correlation between independent variables and dependent variables and the normality of residuals of cloud image method. Finally, taking a continuous beam bridge as an example, the time history analysis of the whole bridge model is carried out to verify whether the variables before and after the correction meet the normal distribution, and the effectiveness of the improved method is evaluated; By establishing the vulnerability curve of the cloud image method and the improved method, the cloud image method and the improved method are evaluated. The results show that the introduction of Box–Cox transformation and 3-sigma criterion can improve the linearity and normality of the probabilistic seismic demand model, and ensure the accuracy of the vulnerability calculation results. Using the Latin hypercube sampling method to consider the uncertainty of the structure can make the vulnerability results more realistic.

Keywords: bridge engineering, improve the cloud image method, Latin hypercube sampling, probabilistic seismic demand model, vulnerability analysis

[1]Eng., CCCC Second Highway Consultants Co., Ltd., Chuangye Road, 430056 Wuhan, China, e-mail: luwhut@163.com, ORCID: 0009-0007-4172-0652
[2]Eng., CCCC Second Highway Consultants Co., Ltd., Chuangye Road, 430056 Wuhan, China, e-mail: cucy@foxmail.com, ORCID: 0009-0004-6671-568X
[3]Associate Prof, Naval University of Engineering, Wuhan 430033, China, e-mail: hf2013beibei@163.com, ORCID: 0009-0003-5296-5453
[4]Eng., Wuhan Longfang Engineering Technology Co., Ltd., Wuhan, Hubei, 430034, China, e-mail: shuang.wang@ksj.com.cn, ORCID: 0009-0007-1702-2934
[5]Eng., CCCC Second Highway Consultants Co., Ltd., Wuhan 430056, China, e-mail: ly_7086@126.com, ORCID: 0009-0004-7079-7411
[6]Eng., CCCC Second Highway Consultants Co., Ltd., Wuhan 430056, China, e-mail: deadeazoe@hotmail.com, ORCID: 0009-0003-9911-2060

1. Introduction

Seismic vulnerability analysis can predict the seismic performance of engineering structures from the perspective of probability, so it is widely used. At present, there are mainly expert scoring methods, historical experience statistics methods [1], and numerical analysis methods [2]. With the rapid development of computer technology, the numerical analysis method is the most widely used. The commonly used numerical analysis methods of seismic vulnerability include incremental dynamic analysis (IDA) [3], strip method [4], and cloud image method [5]. Among them, the IDA method is the most widely used. However, this method involves amplitude modulation or secondary processing of ground motion records, resulting in large calculation errors and calculation amounts. The original ground motion records are used for calculation in the cloud chart method, which avoids the above problems and can quickly obtain the theoretical fragility curve of the structure [6–9].

It is found that when the cloud chart method is used to establish the probabilistic seismic demand model for seismic vulnerability analysis, three basic assumptions are made for the convenience of calculation: (1) The engineering demand parameters at a specific ground motion intensity level obey the lognormal distribution; (2) Linear correlation between ln(IM) and ln(EDP); (3) The variance of ln (EDP) under different IM does not change. Studies have shown that the above three assumptions are inconsistent with reality [10, 11]. Hypothesis (1) has a more serious impact on the calculation results of the vulnerability curve than the latter two. At present, how to improve the theoretical vulnerability analysis method so that it can meet the three basic assumptions and maintain the advantages of fewer analysis times has become an urgent problem to be solved in theoretical vulnerability analysis. The research shows that the quadratic polynomial regression analysis of the least square method [12], incremental dynamic analysis (IDA) [3, 13], Box–Cox transformation [14], and other methods (such as the 3-sigma criterion) are introduced into the cloud image method, and the Box–Cox transformation is combined with Bayesian reasoning for vulnerability analysis [15], which can improve the linearity and normality of the cloud image method. However, the above method will lead to a sharp increase in calculation time. Some scholars have proposed to use Monte Carlo sampling to solve [14], but Monte Carlo sampling re-simulation requires a large number of samples, and the calculation efficiency is low, and the Latin hypercube sampling method is a good choice.

2. Improvement of cloud image method

2.1. Calculation method of traditional cloud image method

The main content of the cloud image method is to establish a probabilistic seismic demand model (PSDM) through the randomness of earthquakes. Cornell et al. [16] proposed to obtain the relationship between EDP and IM according to PSDM, and then combined with the seismic capacity of the structure to solve the damage probability of the structure under different IM to obtain the vulnerability curve. This method assumes that the EDP at a specific ground motion intensity level obeys the lognormal distribution, uses Ordinary Least Squares (OLS) to fit the

regression model, and assumes the relationship between ln(EDP) and ln(IM).

$$\ln(\mathrm{EDP}) = \mathrm{a} + \mathrm{b}\ln(\mathrm{IM}) + \mathrm{e}, \quad \mathrm{e} \sim \mathrm{N}(0, \beta_{\mathrm{EDP}}/\mathrm{IM}). \tag{2.1}$$

where a, b is the regression coefficient.

From the Eq. (2.1), the damage probability Eq. (2.2) under a limit state is obtained.

$$P_f = P(DI \geq LS/\mathrm{IM}) = 1 - \Phi\left(\frac{\ln(LS) - \ln\left(a + b\ln(\mathrm{IM})\right)}{\beta_{\mathrm{EDP}}/\mathrm{IM}}\right) \tag{2.2}$$

where DI is the component requirements; LS is the limit state of component damage; $\Phi(\cdot)$ is a standard normal distribution; $\beta_{\mathrm{EDP}}/\mathrm{IM}$ logarithmic standard deviation for component requirements.

If it is assumed that the seismic capacity C of the component in a certain damage limit state (LS_j) obeys the logarithmic normal distribution with the mean value of S_c and the logarithmic standard deviation of β_c, the damage probability Eq. (2.3) in a certain limit state is obtained.

$$P(LS_j/\mathrm{IM}) = \Phi\left[\frac{\ln(a + b\ln(\mathrm{IM})) - \ln(S_c)}{\sqrt{\beta_D^2 + \beta_c^2}}\right] \tag{2.3}$$

From Eq. (2.1), (2.2), and (2.3), to calculate the damage probability, the cloud image method usually needs to assume that ln(EDP) satisfies the normal distribution, and ln(PGA) and ln(EDP) are linear, where PGA is peak acceleration. However, when the assumption is contrary to the actual situation when ln(EDP) does not satisfy the normal distribution, the calculation results of Eq. (2.2) and (2.3) will be unsatisfactory, which will reduce the reliability of component vulnerability calculation.

2.2. Modification based on BOX-COX transformation

In 1964, Box et al. [17] proposed the Box–Cox transformation, which is widely used in regression analysis. The Box–Cox transformation is to determine the data transformation form by estimating the parameters of the data itself so that the regression model satisfies the normality, linearity, and homoscedasticity. Its general form is:

$$y(\lambda) = \begin{cases} \dfrac{y^\lambda - 1}{\lambda}, & \lambda \neq 0 \\ \ln(y), & \lambda = 0 \end{cases} \quad \text{or} \quad y = \begin{cases} (1 + \lambda y(\lambda))^{\lambda^{-1}}, & \lambda \neq 0 \\ \exp(y(\lambda)), & \lambda = 0 \end{cases} \text{(reverse transformation)} \tag{2.4}$$

where $y(\lambda)$ a new variable after Box–Cox transformation; y is the original variable; λ is the transformation parameter.

The Box–Cox transformation is introduced into Eq. (2.1), and the dependent variable ln(EDP) is improved to update it to a Box–Cox regression model that satisfies normality, linearity, and equal variance assumptions. Currently, the relationship between ln(EDP) and ln(IM) is:

$$\ln(\mathrm{EDP})^\lambda = a' + b'\ln(\mathrm{IM}) + e, \quad e \sim N(0, \beta'_{\mathrm{EDP}}/\mathrm{IM}) \tag{2.5}$$

Since the residual after the transformation conforms to the normal distribution, the parameter λ of the undetermined transformation can be estimated by the maximum likelihood method to find the best value. From $\ln(\mathrm{EDP})^{\lambda} \sim N(a + b\ln(\mathrm{IM}), \beta'_{\mathrm{EDP}}/\mathrm{IM})$, let $x(\lambda) = \ln(\mathrm{EDP})^{\lambda}$, $x = \ln(\mathrm{EDP})$ the probability density of $\ln(\mathrm{EDP})^{\lambda}$ is:

$$f(x) = f(x(\lambda)\cdot J(\lambda, x)) = \frac{1}{\left(\sqrt{2\pi}(\beta'_{\mathrm{EDP}}/\mathrm{IM})^2\right)^n}\cdot \exp\left\{-\frac{1}{2(\beta'_{\mathrm{EDP}}/\mathrm{IM})^2}(x(\lambda) - a' - b'\ln(\mathrm{IM}))^2\right\}\cdot\prod_{i=1}^{n} x_i^{\lambda-1} \tag{2.6}$$

where $J(\lambda, x)$ is the Jacobi determinant.

Taking logarithms on both sides of Eq. (2.6), we can obtain:

$$L(b'\beta'_{\mathrm{EDP}}/\mathrm{IM}, \lambda) = -\frac{n}{2}\ln 2\pi - \frac{n}{2}\ln(\beta'_{\mathrm{EDP}}/\mathrm{IM})^2 + - \frac{1}{2\sigma^2}(x(\lambda) - (x(\lambda) - a' - b'\ln(\mathrm{IM}))^2 + \sum_{i=1}^{n}(\lambda - 1)x_i \tag{2.7}$$

The transformation parameter λ is fixed, and the partial derivatives of the likelihood function to b' and $\beta'_{\mathrm{EDP}}/\mathrm{IM}$ are set to 0. Then, $L(\lambda)$ is:

$$L(\lambda) = -\frac{n}{2}\ln 2\pi - \frac{n}{2}\ln(\beta'_{\mathrm{EDP}}/\mathrm{IM})^2 - \frac{n}{2} + \sum_{i=1}^{n}(\lambda - 1)\ln(x_i) \tag{2.8}$$

Search for the maximum logarithmic likelihood function $L(\lambda)$, draw the $L(\lambda)$ curve, and obtain the best value at the extreme value of the function.

After introducing the Box–Cox transformation, the engineering demand parameter ln(EDP) no longer obeys the original lognormal distribution, and the original damage probability calculation Eq. (2.3) cannoYPICAL CASESt be used. Due to the stratified sampling of variables, the Latin hypercube sampling method will not produce obvious vacancies due to the good uniformity of the sampled samples. Taking the standard normal distribution as an example, which illustrates the differences between MC sampling and LHS sampling. As shown in Fig. 1, R^2 is the coefficient of determination for the fitting effect, and the closer its value is to 1, the better the fitting effect. It can be seen that under the same distribution, MC sampling requires 10000 samples to achieve R^2 above 0.99, while LHS sampling requires 100 samples to achieve this effect; The p-value is the level of significance test for normal distribution. The larger the p-value, the higher the significance level. When the p-value is less than 0.05, it is considered that the variable does not follow a normal distribution. It can be seen that the normality test level of LHS sampling is significantly higher than that of MC sampling. Therefore, under the same conditions, LHS sampling has better results and can achieve the same results as many random samples with fewer sampling times, improving the calculation accuracy.

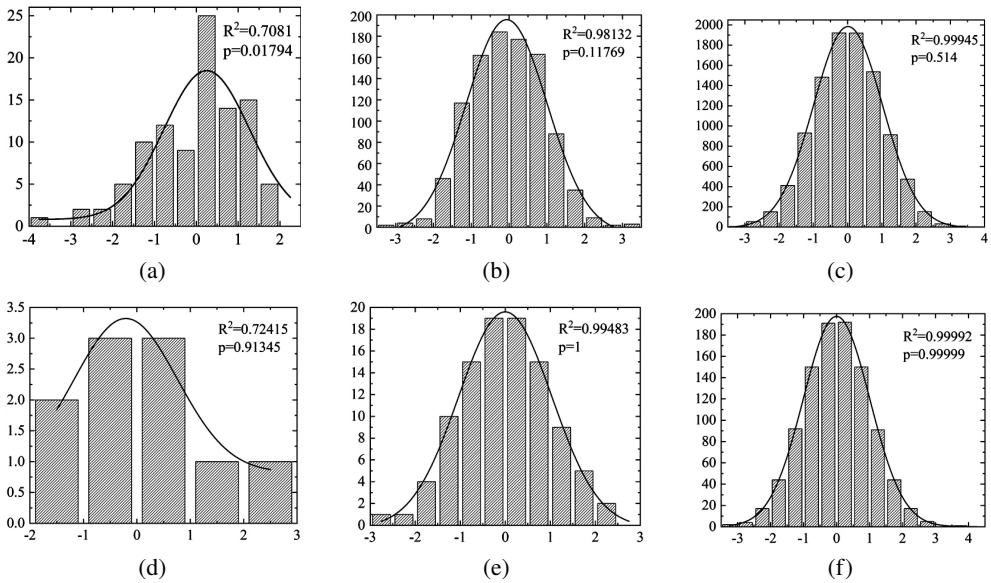

Fig. 1. Probability density distribution map: (a) Monte Carlo sampling 100 times; (b) Monte Carlo sampling 1000 times; (c) Monte Carlo sampling 10000 times; (d) Latin hypercube sampling 10 times; (e) Latin hypercube sampling 100 times; (f) Latin hypercube sampling 1000 times

Taking a one-dimensional vector as an example, assuming m samples are extracted from the vector space, the cumulative distribution function of a continuous random variable is shown in Fig. 2. The steps of Latin hypercube sampling are as follows: first, divide the space vector into m intervals, so that each interval has the same probability, and then randomly select a point in each interval. The selected sample is $(x_1, x_2, x_3, \ldots, x_{m,-1}, x_m)$.

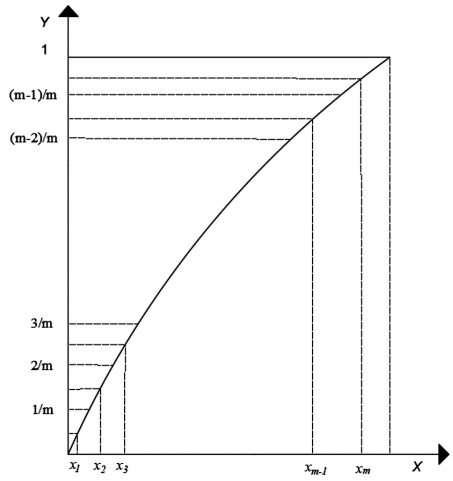

Fig. 2. Schematic diagram of Latin hypercube sampling

Compared with the Monte Carlo sampling method, the sampling efficiency and running time of the Latin hypercube sampling method provide great convenience. Therefore, Box–Cox transformation and Latin hypercube sampling are used to analyze seismic vulnerability. According to this time, in times of Latin hypercube sampling is performed on $\ln(\mathrm{EDP})^{\lambda}$ under each IM according to from $(a' + b' \ln(\mathrm{IM}), \beta'_{\mathrm{EDP}}/\mathrm{IM})$, and the original ln (EDP) value is obtained by inverse transformation Eq. (2.4). At the same time, it is assumed that the capacity of the component (LS_i) obeys the logarithmic normal distribution under the corresponding ultimate damage state. The seismic capacity $\ln(C)$ is also subjected to n Latin cube sampling, and each sampling is judged. The result is expressed by the indicator function:

$$a_i = \begin{cases} 1, & \ln(\mathrm{EDP}) \geq \ln(C) \\ 0, & \ln(\mathrm{EDP}) < \ln(C) \end{cases} \tag{2.9}$$

At this time, the damage probability of the component under LS_i is:

$$P = [LS_j/\mathrm{IM}] = \frac{\sum_{i=1}^{n} a_i}{n} \tag{2.10}$$

where n is the total number of sampling; $\sum_{i=1}^{n} a_i$ is the number of times that the demand value is greater than the capacity value.

2.3. Modification based on 3-sigma criterion

The 3-sigma criterion, also known as the standard deviation method, is usually used to process data with normal distribution or approximate normal distribution. This method is suitable for the case of more data. Statistically, the percentage of the average value less than one standard deviation, two standard deviations, and three standard deviations is 68.27%, 95.45%, and 99.73%, respectively. The standard deviation can reflect the degree of dispersion of the factor, which is based on the average value of the factor. In the process of outlier processing, the average value and standard deviation of the factor are calculated first, and then the parameter m is determined, to determine the reasonable range of the factor value $[\mu - m, x + m]$, and adjust the factor value.

The principle of the 3-sigma criterion can be simply described as follows: If the data obeys the normal distribution, if the deviation from the mean value exceeds three times the standard deviation, these data are outliers, which can be expressed as:

$$P(|x - \mu| > 3\sigma) \leq 0.003 \tag{2.11}$$

where μ is the mean; σ is the standard deviation.

Through the calculation method of the 3-sigma criterion, the engineering demand parameters (ln(EDP)) that do not meet the normality are removed, and some outliers are removed to make ln(EDP) meet the normal distribution. At this time, the damage probability of the structure is calculated by combining the traditional cloud diagram method Eq. (2.1), (2.2) and (2.3), and the vulnerability curve is obtained.

3. Typical cases

3.1. Case overview

In this paper, a continuous beam bridge is taken as the research object. The design bridge length of a bridge is 250 m, the net width of the bridge deck is 12.5 m, and the span arrangement form is (65 + 120 + 65) m. The upper structure of the bridge adopts a continuous box girder, and the lower pier adopts a thin-walled pier. The number of piers is 0#–3# from left to right, and the overall layout of the bridge is shown in Fig. 3.

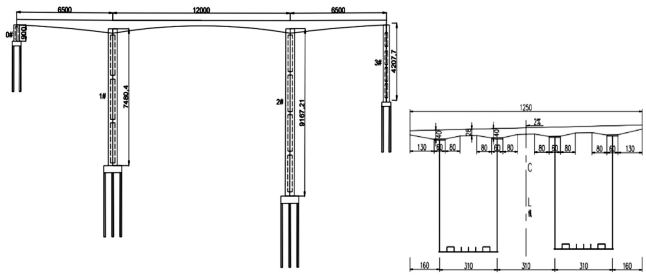

Fig. 3. General layout of the bridge

The finite element 3D model of the whole bridge, which has 150 nodes and 142 elements, is established by the OpenSees program, as shown in Fig. 4. The main girder is simulated by a linear beam-column element (Cross-sectional area is 1.23–1.6 m^2, torsional moment of inertia is 0.03–0.05 m^4, Z-axis bending moment of inertia is 1.23–6.7 m^4, and Y-axis bending moment of inertia is 14.7–19 m^4). The corresponding finite element model is selected according to the failure mode of the pier. The simulation of the bridge pier adopts the Nonlinear Beam-Column Element in OpenSees, and its section adopts the fiber section in OpenSees. The fiber section can divide the section into several small fiber elements, and each section can be assigned a different material constitutive model. The concrete constitutive model is Concrete 01, and steel 01 is used. The pile-soil interaction is simulated by soil spring. In this paper, only the springs in two directions of the horizontal plane are considered, and the spring stiffness is calculated by the m method.

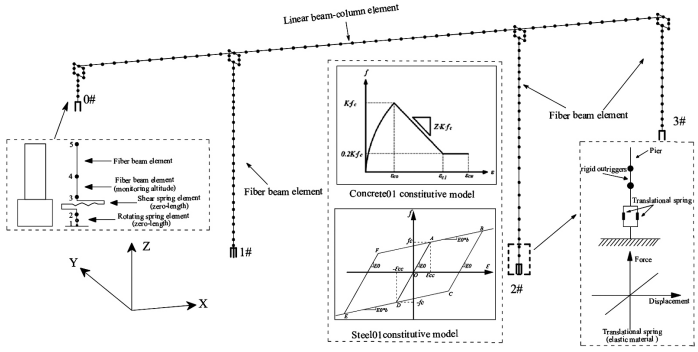

Fig. 4. Diagram of finite element model

For the simulation of the pier, the two-stage kNN (That is k-nearest neighbors) method is used to distinguish the failure mode of the pier, and the seismic failure mode of each pier of the model is obtained [18]. According to different failure modes, the corresponding finite element model is established. The discriminant steps are as follows: (1) Calculate the maximum bending moment value of the pier section; (2) Calculate the shear demand of the pier section; (3) According to the "Specifications for Seismic Design of Highway Bridges (JTG/T 2231-01-2020)" [19], the shear capacity of the section is obtained. (4) According to the cross-section information, the seismic failure mode is identified. The failure modes of each pier are shown in Table 1.

Table 1. Basic design parameters and seismic failure modes of piers

Serial number	V_p/V_n	n	λ	α_l	α_v	ξ	s/h_0	Failure mode
No. 0 Pier	0.84	0.08	1	0.24	0.51	9	0.0169	Shear failure
No. 1 Pier	1.03	0.1	11.6	0.23	0.61	8.7	0.0169	Bending failure
No. 2 Pier	1.03	0.1	14.5	0.23	0.67	6.3	0.0169	Bending failure
No. 3 Pier	0.84	0.08	6.3	0.24	0.54	8.7	0.0169	Bending failure

Note: V_p is the shear demand; V_n is the shear capacity; n is the axial compression ratio; α_l longitudinal reinforcement parameters; α_v is a stirrup parameter; ξ is the relative amount of longitudinal stirrup; s is the stirrup spacing; h_0 is the effective height of the cross-section.

It can be seen from Table 1 that the bending failure of No. 1 pier, No. 2 pier, and No. 3 pier is simulated by fiber beam element. The shear failure of the No. 0 pier was simulated by the simulation method provided in [20], as shown in Fig. 3.

3.2. Selection of indicators

The intensity indexes of earthquakes include peak ground acceleration (PGA), spectral acceleration (IS), and spectral intensity (SA). Since most of the seismic codes in China are based on the fortification intensity, PGA can be obtained from the ground motion parameter zoning in China (GB18306-2001), and most of the ground motion parameters used in vulnerability studies are PGA, the theory is more mature. This paper selects PGA as the ground motion parameter.

The commonly used damage indexes of bridge piers are curvature ductility coefficient, bending ductility coefficient, pier top drift rate, Park-Ang index, residual displacement drift rate, displacement ductility ratio, demand capacity ratio, etc. The pier with bending failure makes it easy to form a plastic hinge and presents good ductility and energy dissipation capacity, so displacement can be used to describe the damage state. The ductility and energy dissipation capacity of shear failure is very poor, and it is unreasonable to choose deformation to describe its damaged state. Therefore, in this paper, the drift rate of the pier top is selected as the damage index of the bending failure pier, and the capacity demand ratio is selected as the damage index of the shear failure pier. The mean and logarithmic standard deviation of drift rate and capacity demand ratio are shown in Table 2 and Table 3 [21].

Table 2. Mean and logarithmic standard deviation of pier top drift rate

LS_1		LS_2		LS_3		LS_4	
μ	σ_1	μ	σ_1	μ	σ_1	μ	σ_1
0.5%	0.25%	1.0%	0.25%	2.0%	0.46%	2.5%	0.46%

Note: LS_1 is the minor injury; LS_2 is the moderate damage; LS_3 is the s serious injury; LS_4 is the complete damage l; μ is the mean value; σ_1 is the logarithmic standard deviation.

Table 3. Mean and log standard deviation of requirement capacity ratio

LS_1		LS_2		LS_3	
μ	σ_1	μ	σ_1	μ	σ_1
1	0.246	2	0.246	3	0.472

3.3. Selection of ground motion

The randomness of ground motion is strong, and different seismic waves have a great influence on the vulnerability curve of the structure [22]. Therefore, this paper selects 100 seismic waves to analyze the vulnerability of the structure. The thickness of the overburden layer in the bridge site area of this bridge is greater than 5 m, the bridge engineering site category is Class II, the earthquake magnitude of the bridge is $M = 7$, and the bridge fault distance is $R_{jb} = 25$ km. According to the bridge site information, the selection steps of seismic waves are as follows: Firstly, according to the V_{30} conversion formula given by Boore [23], the average shear wave velocity V_{30} in the range of 30 m depth of China's Class II site is obtained. Then, 100 seismic waves are selected from the NGA-West2 strong earthquake database according to $M = 6 - 8$, $V_{30} = 366$–450 m/s, $R_{jb} = 0$–100 km [24]. The sequence number, event name, recording site, year, magnitude, fault distance (km), and V_{30} (m/s) information of ground motion records are shown in Table 4. Due to space reasons, this article only lists the first five ground motion information. The 100 ground motion time histories are input according to the longitudinal bridge direction to obtain the response of each component of the structure.

Table 4. Vibration record information sheet

RSSequence number + Event name + Recording site	**Year**	***M***	***R_{jb}* (km)**	***V_{30}* (m/s)**
RSN15_KERN_TAF111	1952	7.36	38.4	385
RSN28_PARKF_C12320	1966	6.19	17.6	409
RSN64_SFERN_FTJ090	1971	6.61	59.5	394
RSN70_SFERN_L01111	1971	6.61	22.2	425
RSN79_SFERN_PAS090	1971	6.61	25.5	415

4. Seismic vulnerability analysis

4.1. Structural random parameters

In this paper, the Latin hypercube sampling method is used to consider the uncertainty of structural parameters, and 100 structure samples are generated by Latin hypercube sampling. From the peak compressive strength of the core concrete (f_c), the strain corresponding to the peak compressive strength (ε_c), the ultimate compressive strength (f_u), the ultimate strain corresponding to the ultimate strength (ε_u); the mass density of concrete (ρ_s); the peak compressive strength (f_c), the strain corresponding to the peak compressive strength (ε_c), the ultimate compressive strength (f_u), and the ultimate strain corresponding to the ultimate strength (ε_u) of the protective layer concrete; the parameters such as the yield stress (f_y), the elastic modulus (E_0) and the yield stiffness ratio (b) of the steel bar consider the randomness of the structure [25, 26] and the detailed information is shown in Table 5. Due to the large number of samples, this paper only lists five structure samples, as shown in Table 6.

Table 5. The probability distribution of random parameters of the structure

Member	Sign	Distribution	Mean value	Coefficient of variation	Lower bound	Upper bound
Cover concrete	f_c/(MPa)	Lognormal	39.5	0.2	27.5	52.5
	ε_c/ (–)	Lognormal	0.002	0.2	0.0013	0.0029
	f_u/(MPa)	Lognormal	7.9	0.2	6.0	10.0
	ε_u/ (–)	Lognormal	0.004	0.2	0.003	0.0054
Core concrete	f_c/(MPa)	Lognormal	51.35	0.2	34	72
	ε_c/ (–)	Lognormal	0.0026	0.2	0.0018	0.0038
	f_u/ (MPa)	Lognormal	10.27	0.2	7.8	13.5
	ε_u/ (–)	Lognormal	0.02	0.2	0.017	0.023
Module density	P_s/ (g·cm^{-3})	Lognormal	2.55	0.2	2.2	2.9
Steel reinforcement	F_y/(MPa)	Lognormal	500	0.1	450	550
	E_0/ (MPa)	Lognormal	2×10^5	0.033	1.79×10^5	2.18×10^5
	b/ (–)	Lognormal	0.007	0.2	0.0059	0.0084

Table 6. Structure samples

Serial number	Cover concrete				Core concrete				Module density	Steel reinforcement		
	f_c (MPa)	ε_c (10^{-5})	f_u (MPa)	ε_u (10^{-5})	f_c (MPa)	ε_c (10^{-5})	f_u (MPa)	ε_u (10^{-5})	P_s (g· cm^{-3})	F_y (MPa)	E_0 (GPa)	b (10^{-5})
1	37	214	7	413	55	301	8	1869	2.712	518	195	791
2	30	239	7	495	61	234	11	2000	2.711	486	212	746
3	29	259	9	359	42	320	8	2179	2.849	473	184	790
4	35	265	6	388	61	226	9	2003	2.597	490	206	607
5	28	143	8	310	64	281	11	1914	2.799	483	198	812

4.2. Vulnerability curve comparison

A series of scatter points (ln(PGA), ln(EDP)) are obtained by taking the logarithm of the peak ground acceleration PGA and the drift rate of the pier top. In this paper, the results of the No.0 pier are selected for a detailed description.

The significance test of ln(EDP) of No. 0 pier was carried out, and the significant level $p < 0.05$ was obtained, which indicated that ln(EDP) did not meet the normal distribution. Box–Cox transformation and 3-sigma criterion were used to process ln(EDP). The significance of the dependent variable and the correlation between the independent variable and the dependent variable are shown in Table 7. After Box–Cox transformation and 3-sigma criterion treatment, ln(EDP)$^{\lambda}$ and ln(EDP) meet the normal distribution the determination coefficient is increased by 1.3 % and 1.1 % respectively, and the correlation degree is improved. Figures 5–7 are the residual distribution map and the residual frequency distribution histogram. The normality of the residual is improved after processing.

Table 7. Analysis results of each method

Parameter	Cloud method	Box–Cox transformation	3-sigma criterion
p	0.020	0.234	0.228
R^2	0.852	0.863	0.862

Note: $p > 0.05$ that the variable obeys the normal distribution; R^2 is the coefficient of determination. The closer R^2 is to 1, the higher the linear correlation between the independent variable and the dependent variable is.

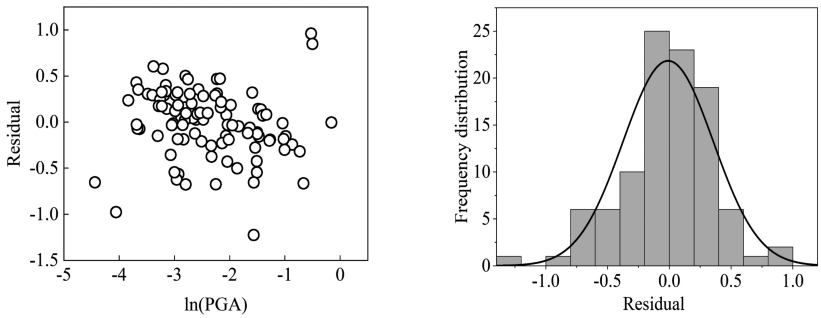

Fig. 5. Analysis results of the cloud image method: (a) Residual distribution map; (b) Residual histogram

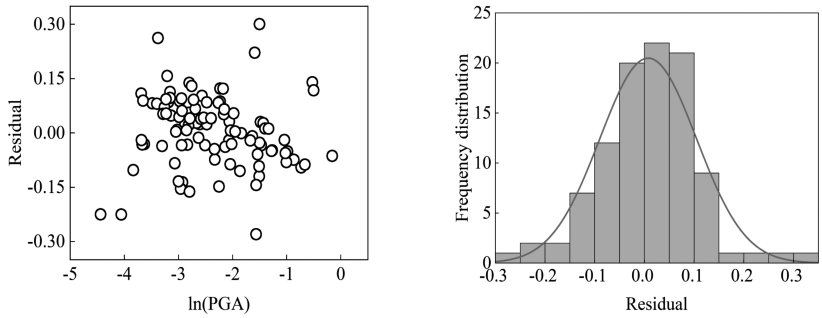

Fig. 6. Results of Box–Cox transformation analysis: (a) Residual distribution map; (b) Residual histogram

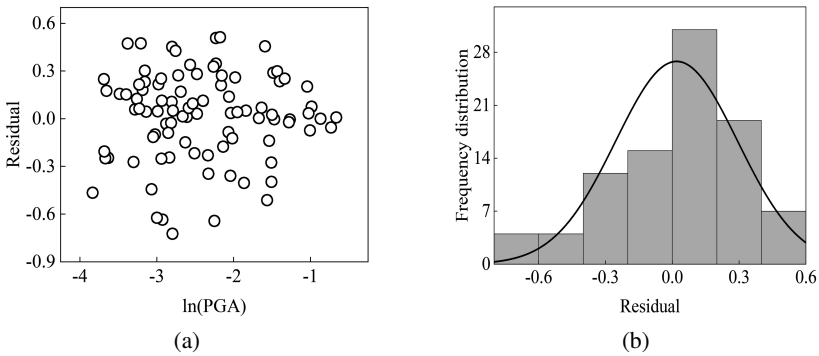

Fig. 7. Analysis results of 3-sigma criterion: (a) Residual distribution map; (b) Residual histogram

The seismic probability demand model of the cloud chart method, Box–Cox transformation, and 3-sigma criterion is established, as shown in Fig. 8. According to the seismic probability demand model, the function expressions of the cloud chart method and the 3-sigma criterion under different damage states are shown in Table 8, where P_f is the damage probability.

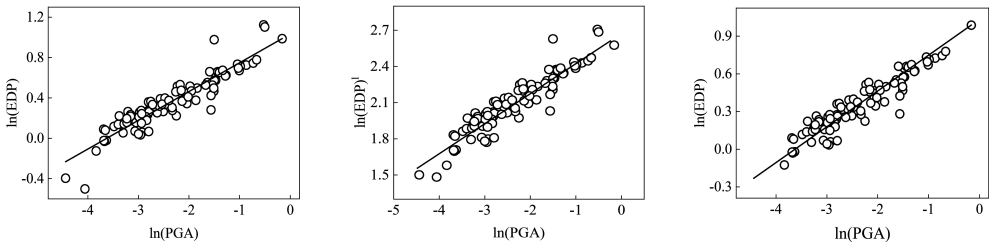

(a) (b) (c)

Fig. 8. Seismic probabilistic demand model: (a) Cloud method; (b) Box–Cox transformation; (c) 3-sigma criterion

Table 8. Function expressions

Vulnerability calculation method	**Damage state**	**Function expressions**
Cloud method	LS_1	$P_f = \Phi\left(\dfrac{0.2851\ln(PGA) + 1.03366 - \ln(1)}{\sqrt{0.168 + 0.060516}}\right)$
	LS_2	$P_f = \Phi\left(\dfrac{0.2851\ln(PGA) + 1.03366 - \ln(2)}{\sqrt{0.168 + 0.060516}}\right)$
	LS_3	$P_f = \Phi\left(\dfrac{0.2851\ln(PGA) + 1.03366 - \ln(3)}{\sqrt{0.168 + 0.060516}}\right)\dfrac{\Delta y}{\Delta x}$
Box–Cox transformation	LS_1	$P_f = \Phi\left(\dfrac{0.2743\ln(PGA) + 1.02144 - \ln(1)}{\sqrt{0.156 + 0.060516}}\right)$
	LS_2	$P_f = \Phi\left(\dfrac{0.27431\ln(PGA) + 1.02144 - \ln(2)}{\sqrt{0.156 + 0.060516}}\right)$
	LS_3	$P_f = \Phi\left(\dfrac{0.2743\ln(PGA) + 1.02144 - \ln(3)}{\sqrt{0.156 + 0.060516}}\right)$

After Box–Cox transformation, Latin hypercube sampling is performed on ln(EDP) under each IM, and ln(EDP) is obtained by Eq. (2.4), and the same sampling times are also performed from ln(C), and the results are obtained according to Eq. (2.11). The Latin hypercube sampling method is used to calculate the exceedance probability, and the different IM damage probabilities are shown in Table 9. According to Table 8 and Table 9, the vulnerability curve is shown in Fig. 9.

Table 9. The damage probability of bridge pier under different *PGA* based on Box–Cox transformation

***PGA*(*g*)**	**LS_1**	**LS_2**	**LS_3**	***PGA*(*g*)**	**LS_1**	**LS_2**	**LS_3**
0.1	0.001	0.000	0.000	0.6	0.974	0.398	0.020
0.2	0.103	0.001	0.000	0.7	0.979	0.552	0.042
0.3	0.385	0.020	0.000	0.8	0.988	0.675	0.080
0.4	0.672	0.100	0.001	0.9	0.986	0.780	0.151
0.5	0.882	0.233	0.005	1.0	1.000	0.858	0.227

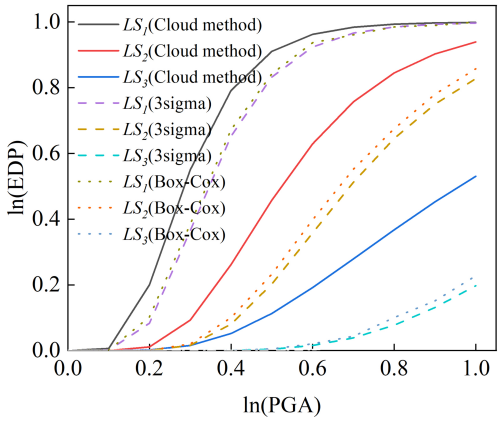

Fig. 9. Vulnerability curves under different vulnerability calculation methods

According to the vulnerability curve, the difference in damage probability between different methods, such as the cloud image method, Box–Cox transformation, and 3-sigma criterion is calculated in Table 10. No. 1 represents the difference in damage probability between the cloud image method and the 3-sigma criterion, No. 2 represents the difference in damage probability between the cloud image method (its data is marked in black, as recommended) and the Box–Cox transformation, and No. 3 represents the difference in damage probability between the 3-sigma criterion and Box–Cox transformation. LS_1, LS_2, and LS_3 represent the "minor", "moderate" and "serious" scenarios, respectively.

Table 10. Damage probability difference of different methods

***PGA*(*g*)**	***LS*$_1$**			***LS*$_2$**			***LS*$_3$**		
	No. 1	**No. 2**	**No. 3**	**No. 1**	**No. 2**	**No. 3**	**No. 1**	**No. 2**	**No. 3**
0.1	0.55%	**0.53%**	0.02%	0.00%	**0.00%**	0.00%	0.00%	0.00%	0.00%
0.2	11.69%	**9.74%**	1.95%	1.02%	**1.02%**	0.00%	0.17%	0.17%	0.00%
0.3	18.50%	**16.50%**	2.01%	7.65%	**7.25%**	0.40%	1.53%	1.53%	0.00%
0.4	13.91%	**11.91%**	2.45%	18.14%	**16.14%**	2.43%	5.14%	5.14%	0.00%
0.5	7.81%	**6.81%**	1.21%	25.51%	**23.51%**	3.00%	10.87%	10.80%	0.07%
0.6	3.86%	**2.56%**	1.30%	27.12%	**22.12%**	4.23%	17.62%	0.00%	0.50%
0.7	1.80%	**2.32%**	0.52%	24.49%	**20.49%**	4.54%	24.01%	0.17%	0.50%
0.8	0.82%	**0.82%**	0.33%	19.97%	**16.97%**	3.16%	29.02%	1.53%	2.35%
0.9	0.37%	**0.77%**	0.43%	15.25%	**12.15%**	3.10%	32.13%	5.14%	2.43%
1.0	0.17%	**0.13%**	0.04%	11.16%	**8.16%**	3.00%	33.29%	10.80%	3.32%

According to Table 10, in the case that ln(EDP) does not satisfy the normal distribution, the vulnerability curve modified by the 3-sigma criterion is compared with the vulnerability curve obtained by the cloud chart method. The maximum difference in damage probability

is 33.2%; after the Box–Cox transformation, the maximum difference in damage probability between the vulnerability curve obtained by the Box–Cox transformation and the vulnerability curve obtained by the cloud image method is 30.29%. When ln(EDP) does not meet the normal distribution, the vulnerability curve obtained by the cloud chart method deviates from the actual situation more seriously, which will lead to an increase in error. After using the 3-sigma criterion and Box–Cox transformation, ln(EDP) or $\ln(EDP)^{\lambda}$ satisfies the normal distribution, the decision regression coefficient (R^2) is also improved, and the distribution of residuals is closer to the normal distribution. After the 3-sigma criterion and Box–Cox transformation, there is a difference between the vulnerability curves obtained by the two improved methods. The maximum damage probability difference is 3.32%. This is because the starting points of the two improved methods are different. However, compared with the error caused by the cloud image method, the difference between the 3-sigma criterion and the Box–Cox transformation is small.

5. Conclusions

1. A seismic vulnerability analysis method combining the Box–Cox transform, 3-sigma criterion, and Latin hypercube sampling is proposed, which solves the problem that the three assumptions of the cloud map method are inconsistent with the reality, and the effectiveness of its application to continuous beam bridge is verified by an example.
2. The Latin hypercube sampling technique is used to consider the uncertainty of structural parameters so that the vulnerability results are more realistic. With the same accuracy, Latin hypercube sampling can greatly reduce the number of samples required for simulation and improve the computational efficiency.
3. The significance level and normality of the regression model after the Box–Cox transformation and the 3-sigma criterion are improved, and the correlation between independent variables and dependent variables is enhanced.
4. The use of the cloud method will lead to the distortion of the calculation results of the structural vulnerability curve; the fragility curves obtained by the Box–Cox transformation and the 3-sigma criterion are very close. The maximum difference in the maximum damage probability is 3.32%. Compared with the cloud image method, the maximum difference between the maximum damage probability after Box–Cox transformation and the 3-sigma criterion is 33.2 %, and the calculation error is improved.

References

[1] M. Kiani, A. Ghalandarzadeh, T. Akhlaghi, and M. Ahmadi, “Experimental evaluation of vulnerability for urban segmental tunnels subjected to normal surface faulting”, *Soil Dynamics and Earthquake Engineering*, vol. 89, pp. 28–37, 2016, doi: 10.1016/j.soildyn.2016.07.012.

[2] V.V. Bertero, “Strength and deformation Capacities of buildings under environments”, *Structural Engineering and Structural Mechanics*, vol. 53, no. 1, pp. 95–102, 1977.

[3] C.G. Lachanas and D. Vamvatsikos, “Rocking incremental dynamic analysis”, *Earthquake Engineering & Structural Dynamics*, vol. 51, no. 3, pp. 688–703, 2022, doi: 10.1002/EQE.3586.

[4] P.A. Conde Bandini, J.E. Padgett, P. Paultre, and G.H. Siqueira, "Seismic fragility of bridges: An approach coupling multiple-stripe analysis and Gaussian mixture for multicomponent structures", *Earthquake Spectra*, vol. 38, no. 1, pp. 254–283, 2022, doi: 10.1177/87552930211036164.

[5] J. Guo, J. Zhong, X. Dang, and W. Yuan "Influence of multidirectional cable restrainer on seismic fragility of a curved bridge", *Journal of Bridge Engineering*, vol. 24, no. 3, art. no. 04018126, 2019, doi: 10.1061/(ASCE)BE.1943-5592.0001352.

[6] J. Jiang, Z. Cheng, C. Xu, and X. Du, "Selection of earthquake records ensembles based on cloud method applied in vulnerability of underground structures", *Journal of Building Structures*, vol. 44, no. 11, pp. 208–215, 2023, doi: 10.14006/j.jzjgxb.2022.0304.

[7] Y. Cao, N. Zhu, X. He, and C. Feng, "Research review and prospect of seismic vulnerability analysis for building structure", *Journal of Jiangxi University of Science and Technology*, vol. 40, no. 6, pp. 01–08, 2019, doi: 10.13265/j.cnki.jxlgdxxb.2019.03.001.

[8] M.A. Billah and S.M. Alam, "Seismic fragility assessment of highway bridges: a state-of-the-art review", *Structure and Infrastructure Engineering*, vol. 11, no. 6, pp. 804–832, 2015, doi: 10.1080/15732479.2014.912243.

[9] J. Zhang and Z. Guan, "Seismic vulnerability analysis of regular continuous girder bridges", *Journal of Vibration and Shock*, vol. 33, no. 20, pp. 140–145, 2014, doi: 10.13465/j.cnki.jvs.2014.20.027.

[10] A. Karamlou and P. Bocchini, "Quantification of the Approximations Introduced by Assumptions on the Marginal Distribution of the Demand for Highway Bridge Fragility Analysis", in *Proceedings of International Conference on Vulnerability & Risk Analysis & Management*. ASCE, 2014, pp. 1321–1330.

[11] K.R. Mackie and B. Stojadinovic, "Comparison of Incremental Dynamic, Cloud, and Stripe Methods for Computing Probabilistic Seismic Demand Models", in *Structures Congress 2005.* ASCE, 2005, pp. 1–11, doi: 10.1061/40753(171)184.

[12] Y. Pan, A.K. Agrawal, and M. Ghosn, "Seismic fragility of continuous steel highway bridges in New York State", *Journal of Bridge Engineering*, vol. 12, no. 6, pp. 689–699, 2007, doi: 10.1061/(ASCE)1084-0702(2007)12:6(689).

[13] J. Zhang and Y. Huo, "Evaluating effectiveness and optimum design of isolation devices for highway bridges using the fragility function method", *Engineering Structures*, vol. 31, no. 8, pp. 1648–1660, 2009, doi: 10.1016/j.engstruct.2009.02.017.

[14] P. Zhang, J. Guo, L. Zhou, and W. Yuan, "Seismic vulnerability analysis of bridge structure based on BOX-COX transformation", *Journal of Vibration and Shock*, vol. 40, no. 1, pp. 192–198, 2021, doi: 10.13465/j.cnki.jvs.2021.01.025.

[15] J. Guo, P. Zhang, and J. Wang, "A novel framework for seismic fragility analysis with the combination of Box–Cox transformation and Bayesian inference", *Engineering Structures*, vol. 277, art. no. 115436, 2023, doi: 10.1016/j.engstruct.2022.115436.

[16] C.A. Cornell, F. Jalayer, R.O. Hamburger, and D.A. Foutch, "Probabilistic basis for 2000 SAC federal emergency management agency steel moment frame guidelines", *Journal of Structural Engineering*, vol. 128, no. 4, pp. 526–533, 2002, doi: 10.1061/(ASCE)0733-9445(2002)128:4(526).

[17] G. Box and D. Cox, "An analysis of transformations", *Journal of the Royal Statistical Society. Series B (Methodological)*, vol. 26, no. 2, pp. 01–06, 1964, doi: 10.1111/j.2517-6161.1964.tb00553.x.

[18] C. Yang, H. Yan, and Z. Dong, "Seismic failure mode identification method of reinforced concrete columns based on KNN algorithm", *Science Technology and Engineering*, vol. 23, no. 25, pp. 10910–10917, 2023.

[19] G. Tang, W. Zheng, and H. Liu, "Brief Introduction to Specifications for Seismic Design of Highway Bridges(JTG/T 2231-01-2020)", *Technology of Highway and Transport*, vol. 37, no. 6, pp. 103–107, 2020.

[20] Z. Sun, C. Chen, B. Si, and D. Wang, "Seismic analysis model considering nonlinear shear effect for RC bridge piers", *Engineering Mechanics*, vol. 32, no. 5, pp. 28–36+50, 2015.

[21] B. Nielson, "Analytical fragility curves for highway bridges in moderate seismic zones", Ph.D. thesis, Georgia Institute of Technology, Atlanta, 2005.

[22] B. Jama, D. Agliz, A. Abderrahman, and M. Derife, "Probabilistic assessment of the seismic vulnerability of a rammed earth construction: a case study", *Archives of Civil Engineering*, vol. 68, no. 2, pp. 325–335, 2022, doi: 10.24425/ace.2022.140645.

[23] D.M. Boore, E.M. Thompson, and H. Cadet, "Regional Correlations of VS30 and Velocites Averaged Over Depths Less Than and Greater Than 30 Meters", *Bulletin of the Seismological Society of America*, vol. 101, no. 6, pp. 3046–3059, 2011, doi: 10.1785/0120110071.

[24] University of California, Berkeley, "PEER Ground Motion Database". [Online]. Available: https://apps.peer.berkeley.edu/products/strong_ground_motion_db.html.

[25] H. Liu, J. Wang, L. Sun, and L. Fan, "Probability characteristics of cross-section capability", *Engineering Mechanics*, vol. 22, no. 06, pp. 104–111, 2005.

[26] Y. Yan and L. Sun, "Multivariate seismic vulnerability analysis of bridges based on Gaussian process regression", *Journal of Vibration and Shock*, vol. 41, no. 23, pp. 27–35, 2022, doi: 10.13465/j.cnki.jvs.2022.23.004.

Received: 2024-04-16, Revised: 2024-07-29